Biophysical Chemistry 253 (2019) 106220

Contents lists available at ScienceDirect

Biophysical Chemistry

journal homepage: www.elsevier.com/locate/biophyschem

Binding of quinazolinones to c-KIT G-quadruplex; an interplay between hydrogen bonding and π-π stacking

Kiana Gholamjani Moghaddam[a], Alex H. de Vries[b], Siewert J. Marrink[b], Shirin Faraji[a,*]

[a] Zernike Institute for Advanced Materials, University of Groningen, Groningen, The Netherlands
[b] Groningen Biomolecular Sciences and Biotechnology Institute & Zernike Institute for Advanced Materials, University of Groningen, Groningen, The Netherlands

GRAPHICAL ABSTRACT

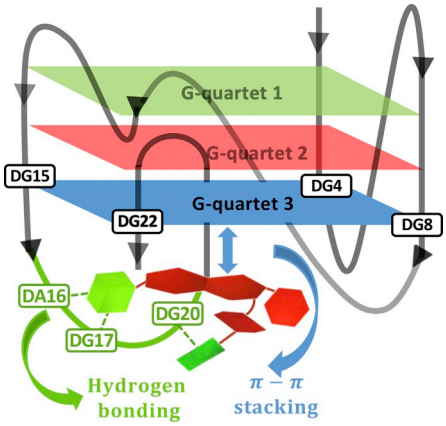

ARTICLE INFO

Keywords:
G-quadruplex
Quinazolinone derivatives
MD simulation
MM-PBSA
Hydrogen bonding
π-π stacking

ABSTRACT

Stabilization of G-quadruplex structures in the c-KIT promoter with the aid of ligands has become an area of great interest in potential cancer therapeutics. Understanding the binding process between ligands and G-quadruplex is essential for a discovery of selective ligands with high binding affinity to G-quadruplex. In the present work, binding mechanisms of 4-quinazolinones to c-KIT G-quadruplex were investigated theoretically by means of molecular dynamics (MD) simulations. To explore the binding affinity of ligands, binding free energy calculations were performed using the molecular mechanics Poisson-Boltzmann surface area (MM-PBSA) method. We demonstrate that the key interactions in G-quadruplex-ligand complexes are π-π stacking and hydrogen bond interactions. However, neither of these two interactions alone determines the stability of the G-quadruplex-ligand complexes; rather, it is the result of an intricate interplay between the two. To further examine the nature of the binding, a free energy decomposition analysis at residue level was carried out. The results clearly demonstrate the crucial roles of two hot spot residues (DG4 and DG8) for the binding of ligands to c-KIT G-quadruplex, and highlight the importance of the planar aromatic moiety of ligands in G-quadruplex stabilization via π-π stacking interactions. Our study can assist in the design of new derivatives of 4-quinazolinone with high binding affinity for c-KIT G-quadruplex.

* Corresponding author.
E-mail address: s.s.faraji@rug.nl (S. Faraji).

https://doi.org/10.1016/j.bpc.2019.106220
Received 9 May 2019; Received in revised form 4 July 2019; Accepted 4 July 2019
Available online 05 July 2019

1. Introduction

In most eukaryotes, the regions of telomere and gene promoters of DNA comprise repeated guanine (G)-rich sequences which are predisposed to self-assemble into non-canonical secondary DNA conformations termed G-quadruplexes [1–3]. Normally, these DNA structures are made up of G-quartets, a cyclic Hoogsteen hydrogen bonding arrangement of four guanine bases, that are stabilized in the presence of K^+ and Na^+ cations [4,5].

Stabilization of G-quadruplex structures formed in the proto-oncogenic c-KIT promoter has attracted growing interests as potential cancer therapeutics [6,7]. It is well established that a variety of malignant cancers such as gastrointestinal stromal tumors (GIST), malignant melanomas, testicular germ cell tumors, pancreatic cancer, etc., are associated with mutation or overexpression of c-KIT [8–12]. Thus, discovery of c-KIT G-quadruplex stabilizers as drug-like candidates has gained enormous attention due to their involvement in inhibition of gene expression [13–16]. Most ligands that stabilize c-KIT G-quadruplex contain planar aromatic core and cationic substituents, thereby enhancing their potential to interact with G-quartets and backbone phosphates, respectively [17–25]. Many scientists have been attempting to design selective interacting ligands that effectively stabilize these structures. Among the different types of ligands, unfused aromatic molecules exhibited high stabilizing ability and binding affinity to c-KIT G-quadruplex [14,26]. One class of the ligands based on this scaffold is 4-quinazolinones. The experimental studies revealed that 4-quinazolinone derivatives not only selectively bind to c-KIT G-quadruplex over duplex DNA, but also suppress transcription or expression of proto-oncogene c-KIT and show GIST cell cytotoxicity [27]. However, questions about the effect of structural variations of the ligands on nature of interactions and G-quadruplex stabilization are still open question. Beyond any doubt, computational methods can help to translate experimental observations into atomic-level mechanistic picture providing detailed insight into the nature of G-quadruplex-ligand interactions. In recent years, a variety of molecular modeling protocols have been utilized to investigate the mechanism of binding between different ligands and G-quadruplex structures [28–32].

Herein, our main focus is to explore the effect of pyrrolidino and piperidino groups, as well as side chains length on the interactions between 4-quinazolinone derivatives (Fig. 1A) and c-KIT G-quadruplex (Fig. 1B) by molecular docking and MD simulations. Molecular docking was used to predict the appropriate site of binding of ligands in G-quadruplex structure. To further dissect the binding mode and illuminate the nature of interactions, MD simulations were performed for each complex obtained from docking calculations. In order to quantify the binding affinities, the free energy analysis based on MM-PBSA approach was used to estimate the stability of G-quadruplex. The latter provides an insight into the main driving forces for interactions between 4-quinazolinone derivatives and G-quadruplex and ultimately stabilization of the complex. Furthermore, the total binding free energy and its energy components for each complex were decomposed to identify the main residues involved in G-quadruplex-ligand interactions and detailed binding mechanisms. We expect that the prediction of interaction profiles of 4-quinazolinone derivatives with c-KIT G-quadruplex at residue level can pave the way to design new ligands with high binding affinity.

2. Computational methods

2.1. Molecular docking

The c-KIT G-quadruplex structure (PDB ID: 2O3M), with the sequence of 5′-AGGGAGGGCGCTGGGAGGAGGG-3′ served as a starting structure in our simulations. The geometry optimizations of all ligands were carried out using Gaussian 03 program [33] at the B3LYP/6-31G* level of theory. Then, binding modes between ligands and G-quadruplex were studied with Autodock Vina program [34]. AutoDockTools was used to add polar hydrogen to the G-quadruplex structure and merge nonpolar hydrogens [35]. Following partial charges were added and rotatable bonds were defined. The active site box with 30 Å × 30 Å × 30 Å dimensions was generated around the G-quadruplex structure to allow ligands to dock to different positions around the G-quadruplex. Finally, the low-energy conformation of each docking was selected for the subsequent MD simulations.

2.2. Molecular dynamics simulations

The MD simulations of ligand-free G-quadruplex and four G-quadruplex-ligand complexes (obtained from molecular docking) were performed using GROMACS 4.6.5 package [36]. The partial charges of ligands were assigned using AM1-BCC method via the ACPYPE tool [37]. Topologies of G-quadruplex and ligands were obtained from Parmbsc0 [38] and Generalized Amber Force Field (GAFF) [39]. The GAFF force field parameters for all ligands are described in Table S1. Two potassium ions were manually added between two G-quartets for the stability of the G-quadruplex. Then, each complex was inserted in a box (dimensions 51 Å × 47 Å × 50 Å) with periodic boundary conditions and solvated with TIP3P [40] water molecules. Then, potassium counterions (the minimum distance between ions is 0.6 nm) were randomly placed throughout the box replacing solvent molecules to neutralize the system. After that, energy minimization of the solvated G-

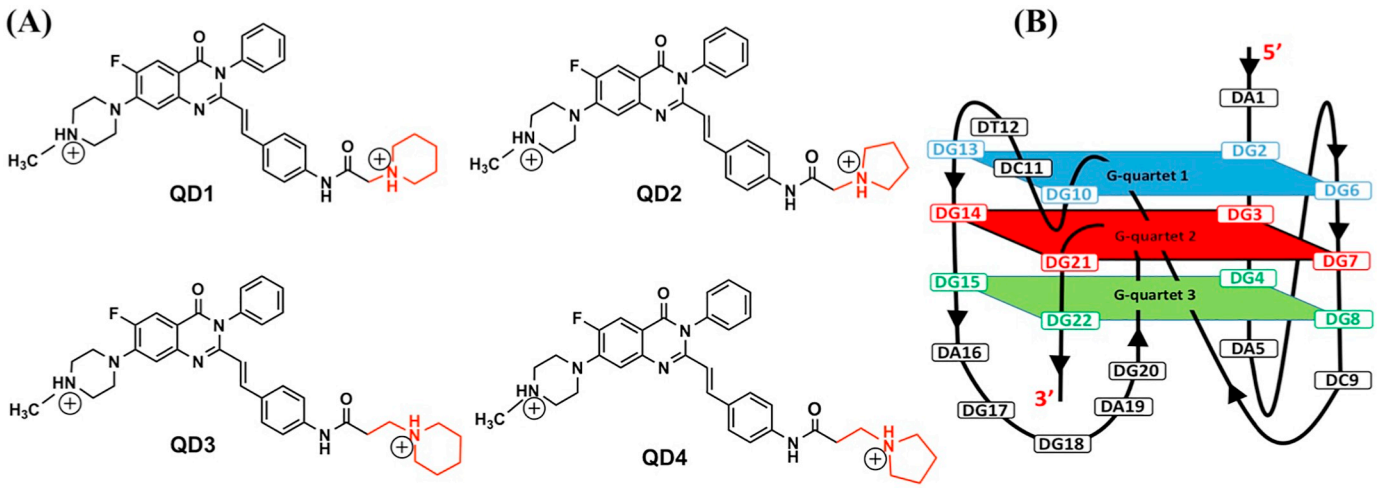

Fig. 1. (A) Chemical structures of 4-quinazolinone derivatives and (B) a schematic representation of c-KIT G-quadruplex investigated in the present study.

quadruplex and G-quadruplex-ligands complexes was calculated using the steepest descent algorithm for 4000 steps. Then, the initial equilibration of the system was performed under an NVT ensemble (300*K*) for 200 ps, continued by 300 ps NPT equilibration (1 bar). The velocity rescaling [41] and Parrinello-Rahman barostat algorithms [42,43] were utilized for temperature and pressure coupling, respectively ($\tau_T = 0.1$, $\tau_p = 1ps$). After equilibrating, four 50 ns MD production runs for each complex (16 MD runs in total) were performed with a time step of 2 fs in which the output files were collected every 2 ps. During the simulation, the long-range electrostatic interactions were calculated using particle mesh Ewald (PME) method [44] and the LINCS algorithm [45] was applied to fix all molecular bonds. Cutoff for the treatment of short-range van der Waals and electrostatic interactions was set to 10.0 Å. Finally, MD trajectory analysis was performed with the programs in the GROMACS 4.6.5 package. Clustering analysis employing the Gromos algorithm [46] was carried out using a cutoff 0.15 nm to obtain the representative structures based on the most populated cluster. All trajectories were visualized by means of the VMD 1.9 [47] program and molecular graphic images were created using the Chimera 1.10 [48] program.

2.3. Free energy analysis

In order to examine binding affinity of ligands to G-quadruplex, MM-PBSA analysis [49–51] was employed via g_mmpbsa tool [52]. For each complex, the binding free energy was calculated based on 100 snapshots extracted from the MD trajectory. A bootstrap analysis (5000 steps) was used to estimate standard errors.

MM-PBSA method calculates the binding free energy ($\Delta G_{binding}$) according to the following equations:

$$\Delta G_{binding} = \Delta G_{vac} + \Delta G_{solv} \quad (1)$$

where, ΔG_{vac} and ΔG_{solv} are the binding free energy in the vacuum and solvent, respectively. The Δ refers to the difference between the complex and G-quadruplex and ligand.

Here, ΔG_{vac} can be expressed as

$$\Delta G_{vac} = \Delta E_{MM} - T\Delta S \quad (2)$$

where, ΔE_{MM} refers to the molecular mechanics potential energy in the vacuum and it is sum of bonded (ΔE_{int}) (bond, angle, and torsional angle energies), and non-bonded, i.e. electrostatic (ΔE_{elec}), and van der Waals energies (ΔE_{vdw}).

$$\Delta E_{MM} = \Delta E_{int} + \Delta E_{elec} + \Delta E_{vdw} \quad (3)$$

In the single trajectory approach, it is assumed that the conformation of G-quadruplex and ligand in the complex and separate G-quadruplex/ligand forms are identical. Thus, ΔE_{int} is zero. $T\Delta S$ is related to the entropy contribution in the gas phase in which T and S are the temperature and entropy, respectively. Note that, the entropy contribution is not considered in the g_mmpbsa tool, and recent study has shown that including entropy makes only a small improvement of free energy in relation to experiment [52].

The solvation free energy (ΔG_{solv}) is composed of polar (ΔG_{ps}) and non-polar (ΔG_{nps}) contributions [53–55]

$$\Delta G_{solv} = \Delta G_{ps} + \Delta G_{nps} \quad (4)$$

$$\Delta G_{nps} = \gamma SASA + \beta \quad (5)$$

In this analysis, an implicit solvent model is used for solvation free energy calculations. The polar contribution is calculated by solving the non-linear Poisson-Boltzmann (PB) equation [55–57]. The nonpolar contribution of solvation free energy is calculated based on Eq. (5), which is related to the solvent accessible surface area (SASA) [54]. In this equation, γ is a constant related to the surface tension of the solvent, and β refers to the fitting parameter. These values were obtained from a least-squares fitting method to a plot of experimental alkane transfer free energies against accessible surface area [58]. For γ and β, several values have been reported in the literature [59]. Here, γ and β are set to be 0.00542 kcal/(mol Å^2) and 0.92 kcal/mol, respectively [60].

2.4. Free energy decomposition

In order to investigate the mechanism of binding between ligands and c-KIT G-quadruplex in detail, free energy decomposition analysis [61] was performed using MM-PBSA decomposition process of g_mmpbsa tool. In this analysis, the binding free energy of each residue is decomposed into contributions from molecular mechanics and solvation energies which can be described in the following equation:

$$\Delta G_{residue} = \Delta E_{MM} + \Delta G_{ps} + \Delta G_{nps} \quad (6)$$

where, ΔE_{MM} is sum of electrostatic and van der Waals energies which are calculated for each residue (recall, ΔE_{int} is zero). The polar and nonpolar contributions of the solvation free energy are determined by PB and SASA models, respectively. The energy components of each residue of c-KIT G-quadruplex were calculated by averaging over 100 snapshots taken from MD simulations.

3. Results and discussion

3.1. Quinazolinones bind to 3′ end of G-quadruplex

Molecular docking studies were performed to decipher the most potent binding sites of all ligands to c-KIT G-quadruplex by setting the whole G-quadruplex as a search space. The results of docking revealed that the favorable binding site for the ligands in the G-quadruplex is the 3′ end of the G-quadruplex structure (G-quartet 3). The two cationic side chains of the ligands were located close to the loop residues (Fig. S1). In addition, there are many studies that showed that in this structure of G-quadruplex, there is a cleft at the 3′ end of G-quadruplex between G-quartet 3 and the loop (A16-G17-G18-A19-G20). This cleft is a unique binding site for ligands because of the sufficient size and its nature [10,62–63].

The data reported in Table 1 indicate that ligand QD1 and QD2 with shorter side chains show slightly higher binding affinity to G-quadruplex structure than other derivatives. This is consistent with the experimental results that the ligand QD1 and QD2 with lower IC_{50} values (1.3 μM and 2.3 μM) reveal more stabilizing effects onto c-KIT G-quadruplex compared to QD3 and QD4 (IC_{50} = 8.2 μM and 13.4 μM) (Table S2) [27].

In order to comprehensively understand the binding modes and nature of interactions between ligands and G-quadruplex, 50 ns MD simulations were carried out on the G-quadruplex-ligand complexes obtained from docking results. It is clear that these ligands with a planar aromatic core and two cationic side chains not only provide π-π stacking interactions with the aromatic surface of G-quartet 3 (DG4 and DG8), but also the side chains can interact with the G-quadruplex loop as it is shown schematically in Fig. 2. The representative structures of the most populated clusters obtained from clustering analysis are depicted in Fig. 3.

Table 1
Comparison of docking binding energies of ligands to G-quadruplex.

Ligand	Binding energy (kcal/mol)
QD1	−8.3 ± 0.2
QD2	−8.0 ± 0.2
QD3	−7.8 ± 0.2
QD4	−7.2 ± 0.2

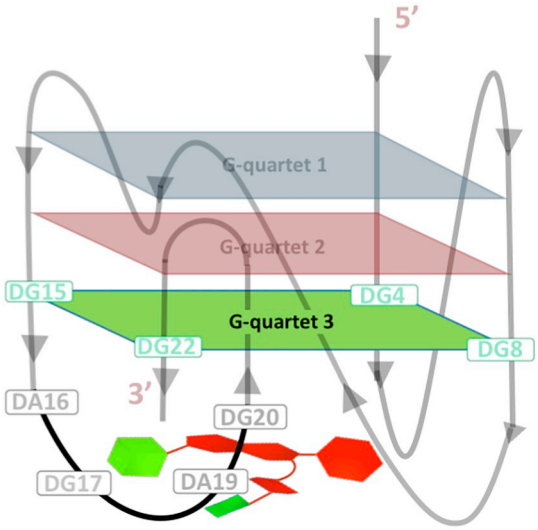

Fig. 2. Schematic representation of binding sites of a ligand in G-quadruplex-ligand complex. Four residues, DA16, DG17, DA19 and DG20 are located at the G-quadruplex loop. The red and light-green surfaces of the ligand explain the aromatic groups and non-aromatic rings of the ligand, respectively. (For interpretation of the references to colour in this figure legend, the reader is referred to the web version of this article.)

3.2. Ligands increase stability of G-quadruplex

To assess conformational stability of each complex during MD simulations, root mean square deviation (RMSD) calculations for all 16 runs were performed on the G-quadruplex with respect to the initial structures. The small RMSDs (Fig. 4 and S2-S5, black plots) represent stability of systems during MD simulations. In addition, the RMSD of G-quartets as a rigid part of the G-quadruplex was calculated against the starting structure (Fig. 4 and S2-S5, blue plots). The RMSDs show that the G-quarters are stable during MD simulations. As evident from Fig. 4 and S2-S5, RMSD variations of G-quadruplex for all complexes are slightly larger than those of G-quartets. This observed difference implies that backbone residues in the G-quadruplex structure are more flexible than rigid G-quartets. To investigate the effect of ligand binding on G-quadruplex stabilization, RMSD of the ligand-free G-quadruplex during 50 ns simulation was calculated. As can be seen in Fig. 4, the average RMSD of the G-quadruplex is slightly larger for ligand-free structure (red plots) as compared to that of each complex, suggesting that the ligands binding slightly enhances stability of c-KIT G-quadruplex.

To further investigate the G-quartets stability due to ligand binding, average hydrogen bond (N2 − H···N7 and N1 − H···O6) (Fig. 5) occupancies between the G-quartets for all G-quadruplex-ligand complexes and ligand-free G-quadruplex were calculated during the entire simulation which are summarized in Table 2. To define a hydrogen bond, cutoff distance (donor-acceptor) and angle (hydrogen-donor-acceptor) of 3.5 Å and 30° have been used, respectively.

As can be seen in Table 2, the hydrogen bonds between G-quartets in all G-quadruplex-ligand complexes are present during > 98.3% of the simulation time. Indeed, the results indicate the stability of systems throughout the MD simulations. Furthermore, these ligands with the average hydrogen bond occupancies in the range of 98.3–98.9% compared to ligand-free G-quartets with average occupancy of 97.4% have a positive effect on G-quartet stabilization and consequently stability of G-quadruplex.

3.3. Ligands bind via both hydrogen bonds and π-π stacking interactions

In order to investigate the binding interactions of the ligands with G-quadruplex, the hydrogen bond and π-π stacking interactions between G-quadruplex and ligands were analyzed over 50 ns simulations. The hydrogen bond analysis was calculated for 16 MD runs as shown in Table 3 and S3. As can be seen in Table 3, each ligand in all MD runs has the same hydrogen bond patterns with G-quadruplex structure. It is clear in Fig. 6 that ligands QD1 and QD3 with a piperidino group at the side chain terminus can form two similar hydrogen bonds with c-KIT G-quadruplex; 1) O4'…H-N22, the NH group of the methylpiperazine ring formed a hydrogen bond with the O4' atom of DG20. 2) O1P…H-N40 (N41 for QD3), the formation of hydrogen bond between piperidino

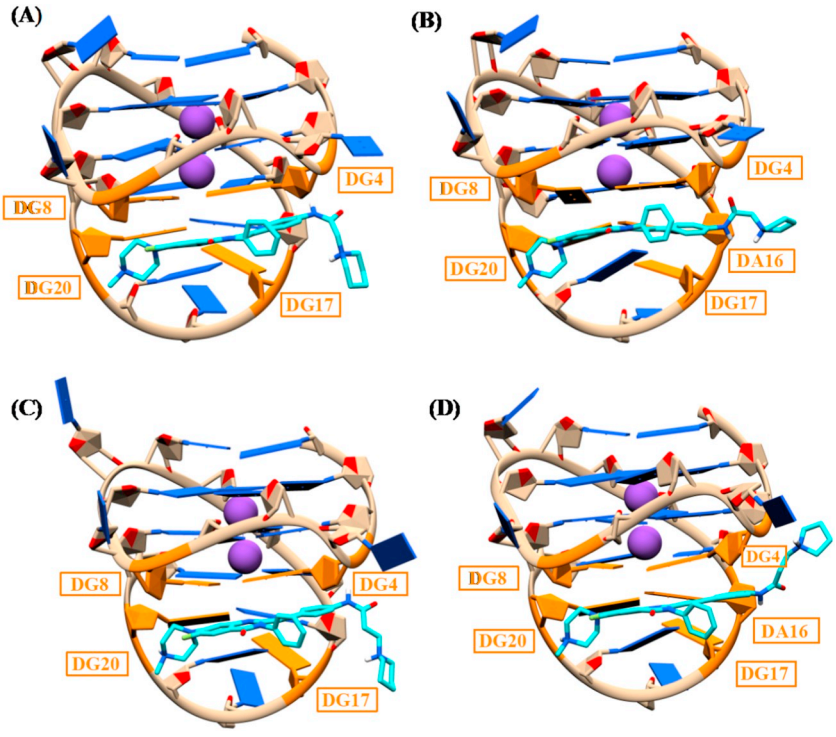

Fig. 3. Representative structures identified via clustering analysis for G-quadruplex in complex with (A) QD1, (B) QD2, (C) QD3, (D) QD4 ligands from MD simulations. All ligands are shown as cyan sticks and the residues involved in binding are indicated in orange colour. (For interpretation of the references to colour in this figure legend, the reader is referred to the web version of this article.)

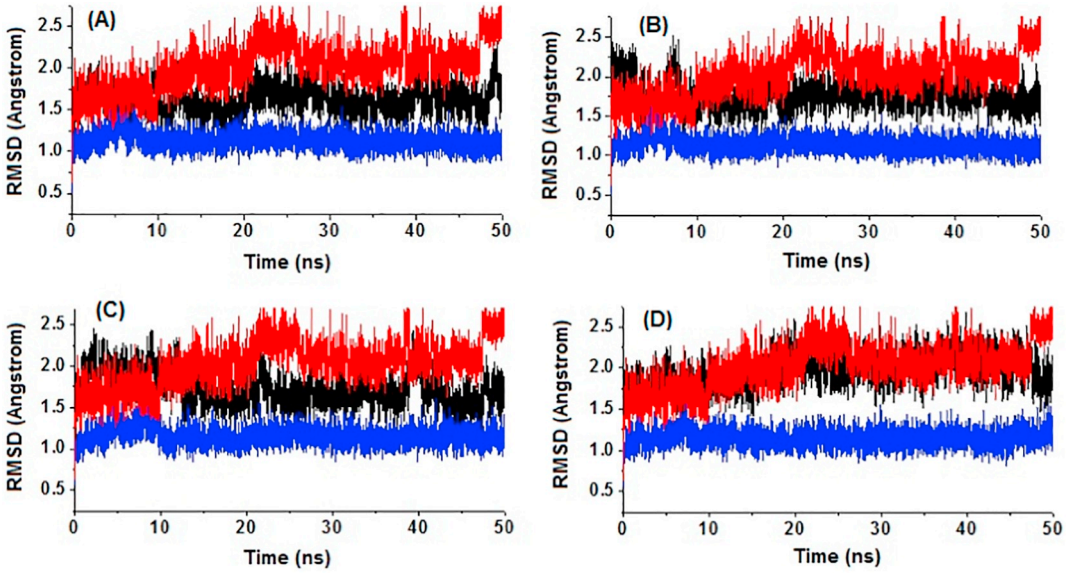

Fig. 4. RMSDs as a function of simulation time of G-quadruplex (black) complexed with (A) QD1, (B) QD2, (C) QD3 and (D) QD4 ligands and ligand-free G-quadruplex (red). The blue indicates the RMSDs for G-quartets complexed with ligands. (For interpretation of the references to colour in this figure legend, the reader is referred to the web version of this article.)

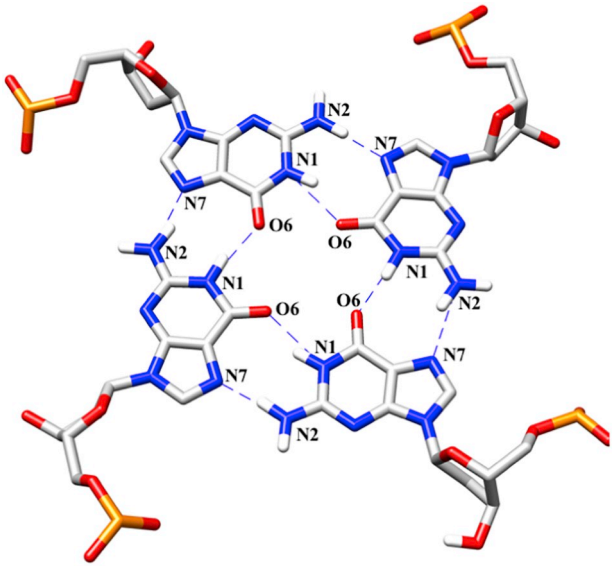

Fig. 5. Hoogsteen hydrogen bond network in each G-quartet.

group and the phosphate oxygen atom of DG17. For ligands QD2 and QD4, the side chains of the ligands were oriented in such a way that four hydrogen bonds with G-quadruplex structure are formed. Three of these hydrogen bonds are similar in nature for QD2 and QD4; 1) O4'…H-N22, similar to QD1 and QD3, the NH group of the methylpiperazine ring formed a hydrogen bond with the O4' atom of DG20. 2 & 3) the hydrogen atom of the −NH−CO− peptide linkage group can form two hydrogen bonds with residue DG17 and DA16 through the oxygen atoms of the sugar-phosphate backbone, O1P and O3' respectively. In addition, the pyrrolidino group of QD4 was positioned close to DG4 that leads to the hydrogen bond formation between the NH group of pyrrolidino ring and the phosphate oxygen atom of DG4 (O2P…H-N41), while the pyrrolidino group of QD2 can be hydrogen bonded to the phosphate oxygen atom of DG17, (O1P…H-N40). It can be seen for the hydrogen bonds presented in Table 3 the occupation fluctuates during simulations, and that their lifetimes differ substantially (Figs. S6-S9).

Table 3
Hydrogen bonds data during 50 ns MD simulations between ligands (LIG stands for ligands) and G-quadruplex over 40.0% of the simulation time. Error bars were obtained from block averaging method.

G-quadruplex in complex with ligand	Hydrogen-donor	Hydrogen-acceptor	Occupancy (%)
QD1	LIG(H46)N40	17 DG (O1P)	47.3 ± 17.3
	LIG(H25)N22	20 DG (O4')	79.1 ± 6.5
QD2	LIG(H45)N40	17 DG (O1P)	51.7 ± 15.9
	LIG(H36)N35	17 DG (O1P)	50.4 ± 8.6
	LIG(H36)N35	16 DA (O3')	51.0 ± 8.2
	LIG(H25)N22	20 DG (O4')	81.5 ± 7.3
QD3	LIG(H47)N41	17 DG (O1P)	94.1 ± 2.1
	LIG(H25)N22	20 DG (O4')	87.1 ± 2.1
QD4	LIG(H46)N41	4 DG (O2P)	96.8 ± 1.7
	LIG(H36)N35	17 DG (O1P)	52.4 ± 19.3
	LIG(H36)N35	16 DA (O3')	77.8 ± 9.9
	LIG(H25)N22	20 DG (O4')	87.6 ± 5.4

Table 2
Average occupancy (%) of Hoogsteen hydrogen bonds in G-quartets during MD simulations. Error bars were obtained from block averaging method [64].

G-quartet	G-quadruplex- ligand complex				Ligand-free G-quadruplex
	QD1	QD2	QD3	QD4	
G-quartet 1 (DG10-DG13-DG2-DG6)	99.6 ± 0.0	99.5 ± 0.1	99.4 ± 0.0	99.3 ± 0.0	99.4 ± 0.0
G-quartet 2 (DG21-DG14-DG3-DG7)	97.7 ± 0.3	97.6 ± 0.2	96.8 ± 0.1	96.4 ± 0.1	94.7 ± 0.1
G-quartet 3 (DG22-DG15-DG4-DG8)	99.5 ± 0.1	99.4 ± 0.1	99.3 ± 0.0	99.2 ± 0.1	98.2 ± 0.4
All G-quartets	98.9 ± 0.1	98.8 ± 0.0	98.5 ± 0.0	98.3 ± 0.0	97.4 ± 0.1

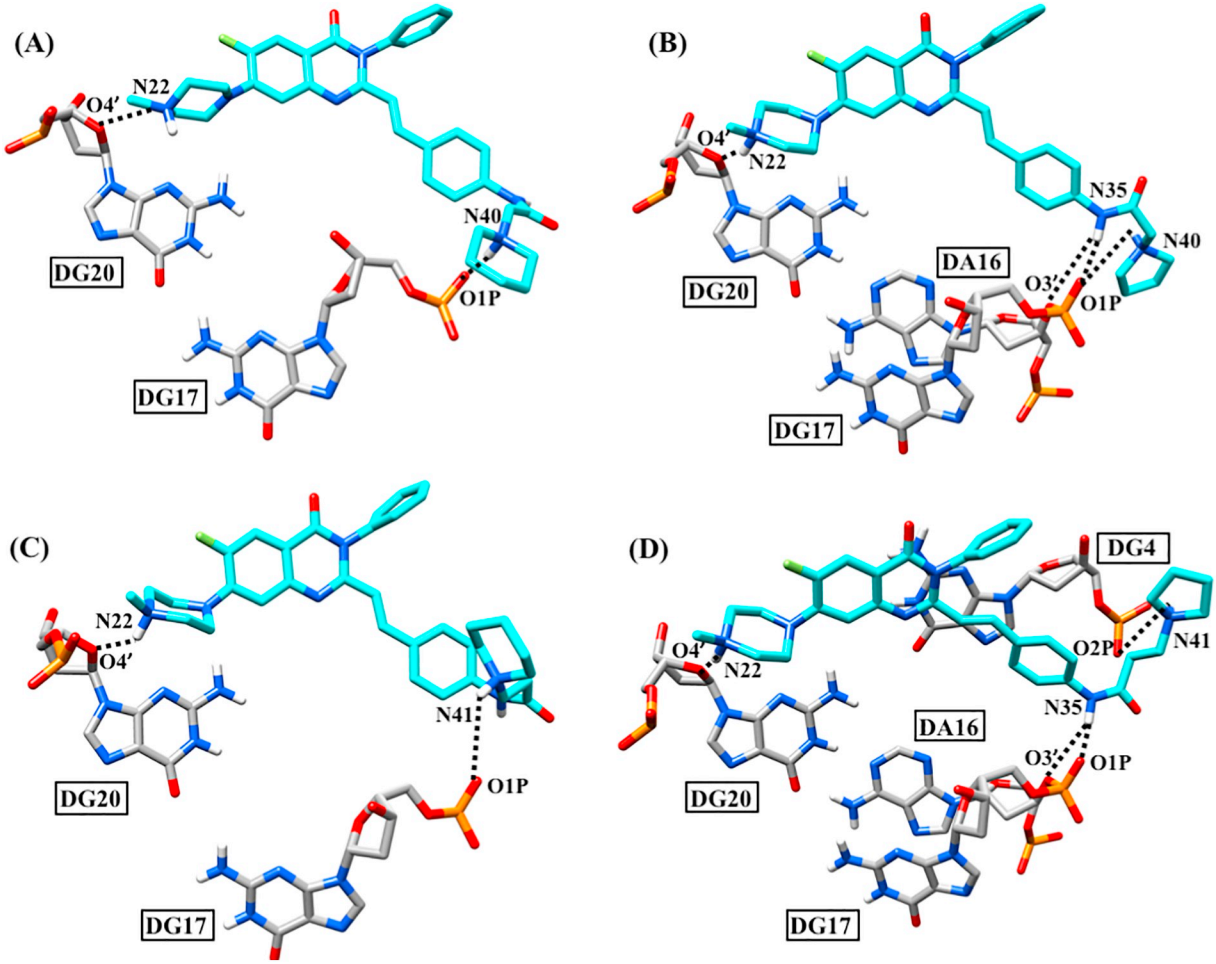

Fig. 6. Hydrogen bonds between (A) QD1, (B) QD2, (C) QD3, (D) QD4 ligands and adjacent residues of G-quadruplex during MD simulations. All ligands are shown as cyan sticks. (For interpretation of the references to colour in this figure legend, the reader is referred to the web version of this article.)

The large error bars for the hydrogen bonds with relatively low occupation reflect the relatively slow fluctuations. The block averaging leads to lower error if the occupation consistently has the same average value over shorter time intervals.

Furthermore, the MD trajectories were analyzed for π-π stacking interactions between ligands and G-quartet 3. The distances between the center of mass of the aromatic rings of the ligands and DG4, DG8 residues (adjacent to the ligands) of G-quartet 3 were calculated during the course of MD simulations (Fig. 7). As it is clear in these figures, all these ligands favor the π-π stacking interactions with DG4 and DG8. In all complexes, the benzene ring of ligands stacks with DG4 (average distance: ~ 4.0 ± 0.0 Å), while their quinazolinone ring stacks with DG8 (average distance: ~ 3.9 ± 0.0 Å), as depicted in Fig. 8.

It must be emphasized here that all the ligands, considered in this work, have two positions for interacting (binding) to G-quadruplex structure; i) π-π stacking interactions between aromatic rings of ligands and G-quartet 3 (Fig. 8), ii) hydrogen bond interactions with the loop of G-quadruplex (see Figs. 2 and 6). Importantly, for the reasons that will be discussed in more detail in the following sections, neither of these two types of interaction alone determines the stability of the G-quadruplex-ligand complex. For example, it is found from Table 3 and Fig. 6 that ligands QD2 and QD4 form more hydrogen bonds (four hydrogen bonds) with G-quadruplex structure than QD1 and QD3 (two hydrogen bonds). However, forming more hydrogen bonds does not necessarily lead to the most stable structure (see section 3.4–5). Indeed, a balance between these two factors is the outcome of G-quadruplex stabilization that will be explain in the following sections.

3.4. Free energy analysis underlines importance of both hydrogen bond and π-π stacking

To investigate and quantify the binding effects of ligands on G-quadruplex stabilization, free energy analysis was performed using the MM-PBSA approach and the results are reported in Table 4. In order to understand information about driving forces in G-quadruplex-ligand interactions, it is essential to investigate contributions of energy components. According to Table 4, in all complexes, the polar solvation energies (ΔG_{ps}) provide unfavorable contributions to the binding free energies, whereas electrostatic (ΔE_{elec}), van der Waals (ΔE_{vdw}) and nonpolar solvation (ΔG_{nps}) interactions promote favorable complex formation. The presence of two cationic side chains assists the ligands to interact with G-quadruplex backbone which contribute to negative electrostatic energies (ΔE_{elec}). The favorable van der Waals contributions (ΔE_{vdw}) can be attributed to π-π stacking interactions between the quinazolinone pharmcophore of ligands and G-quartet 3. As can be seen in Table 4, ΔG_{polar} is sum of the electrostatic (ΔE_{elec}) and polar solvation (ΔG_{ps}) energies that shows a positive value for all ligands, whereas the total nonpolar contribution ($\Delta G_{nonpolar}$) of binding free energy, composed of van der Waals (ΔE_{vdw}) and nonpolar solvation energies (ΔG_{nps}), makes a favorable contribution for all ligands. Therefore, the nonpolar interactions (average ~ −55.2 kcal/mol) between ligands and c-KIT G-quadruplex play a main role in G-quadruplex-ligand binding which is mainly attributed to van der Waals (π-π stacking) interactions.

Furthermore, the affinity of 4-quinazolinone derivatives toward c-KIT G-quadruplex was deduced from the obtained binding free energies

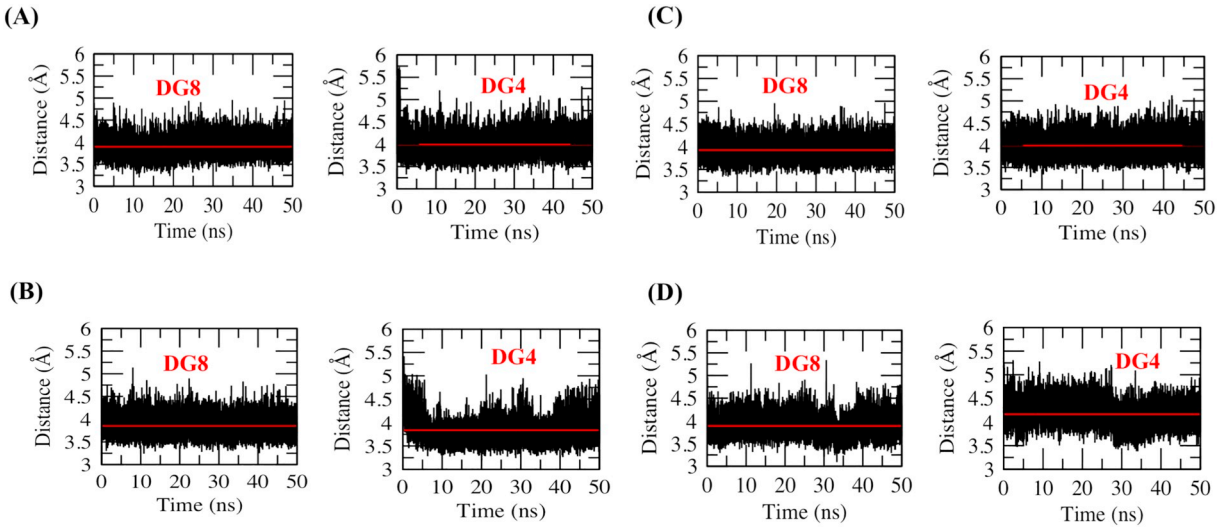

Fig. 7. Stacking distance between the center of mass of quinazolinone ring/benzene ring of ligands and DG8/DG4 during the MD simulations. (A), (B), (C) and (D) refer to ligand QD1, QD2, QD3 and QD4, respectively. The average values are indicated by a red solid line. (For interpretation of the references to colour in this figure legend, the reader is referred to the web version of this article.)

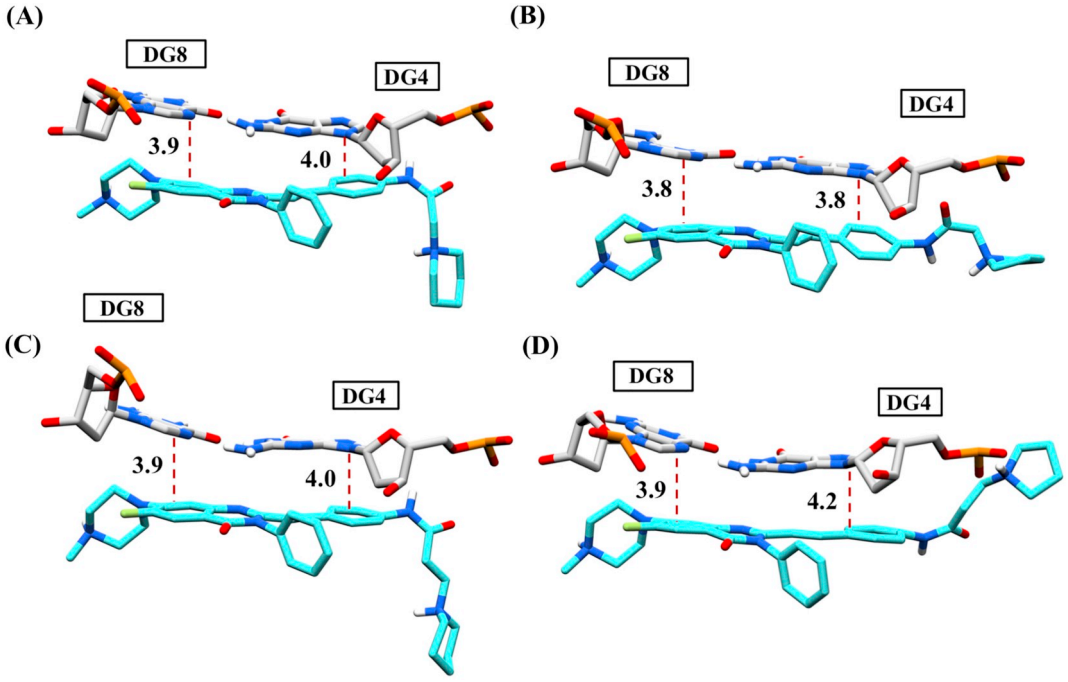

Fig. 8. π-π stacking interactions between aromatic rings of (A) QD1, (B) QD2, (C) QD3, (D) QD4 ligands and DG4 and DG8 in G-quartet 3 during the course of MD simulations. All ligands are shown as cyan sticks. Dashed lines indicate average stacking distances; all distances are given in Å.

Table 4
Binding free energy results for ligands binding to c-KIT G-quadruplex (kcal/mol). Error bars were obtained from the bootstrap analysis.

Ligand	ΔE_{elec}	ΔE_{vdw}	ΔG_{ps}	ΔG_{nps}	ΔG_{polar}	$\Delta G_{nonpolar}$	ΔG_{bind}
QD1	−93.8 ± 1.7	−51.5 ± 1.3	105.2 ± 2.6	−4.1 ± 0.1	11.4 ± 3.1	−55.6 ± 1.3	−44.2 ± 0.8
QD2	−96.7 ± 1.9	−53.9 ± 1.6	112.2 ± 3.3	−4.4 ± 0.1	15.6 ± 3.8	−58.3 ± 1.6	−42.7 ± 0.6
QD3	−91.0 ± 2.1	−48.6 ± 1.6	103.6 ± 3.4	−4.0 ± 0.1	12.7 ± 4.0	−52.7 ± 1.6	−40.0 ± 0.8
QD4	−93.1 ± 2.4	−50.2 ± 1.9	108.7 ± 3.9	−4.3 ± 0.2	15.7 ± 4.6	−54.4 ± 1.9	−38.8 ± 0.7

Note:
$\Delta G_{polar} = \Delta E_{elec} + \Delta G_{ps}$
$\Delta G_{nonpolar} = \Delta E_{vdw} + \Delta G_{nps}$
$\Delta G_{bind} = \Delta E_{elec} + \Delta E_{vdw} + \Delta G_{ps} + \Delta G_{nps}$

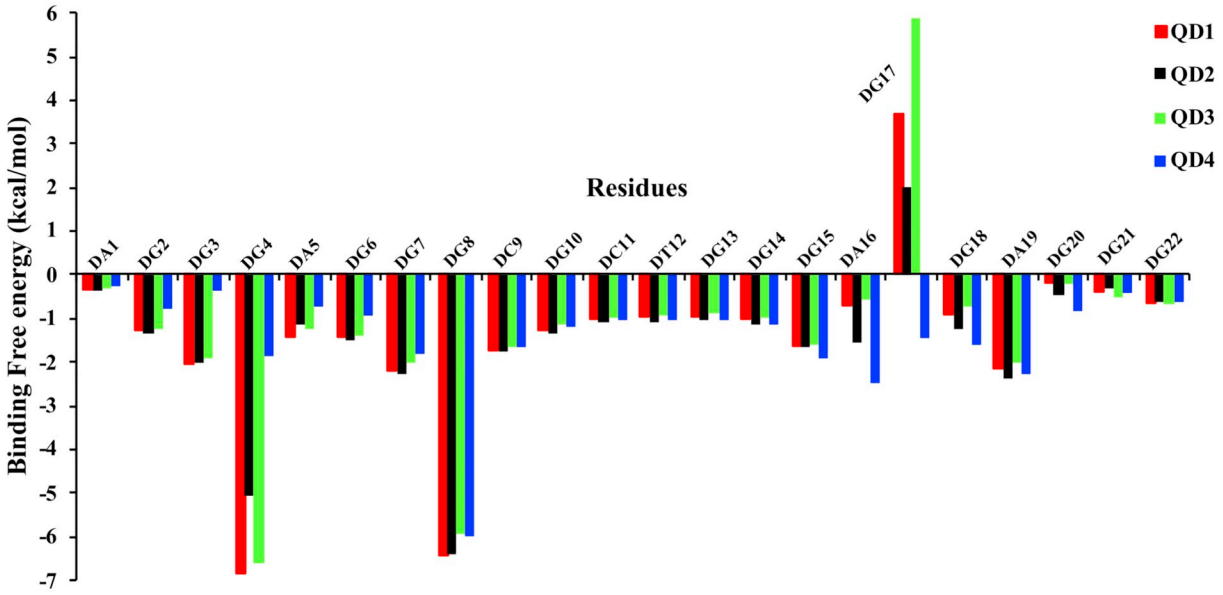

Fig. 9. Free energy decomposition on a per residue level for the complexes. Red: QD1, black: QD2, green: QD3 and blue: QD4. (For interpretation of the references to colour in this figure legend, the reader is referred to the web version of this article.)

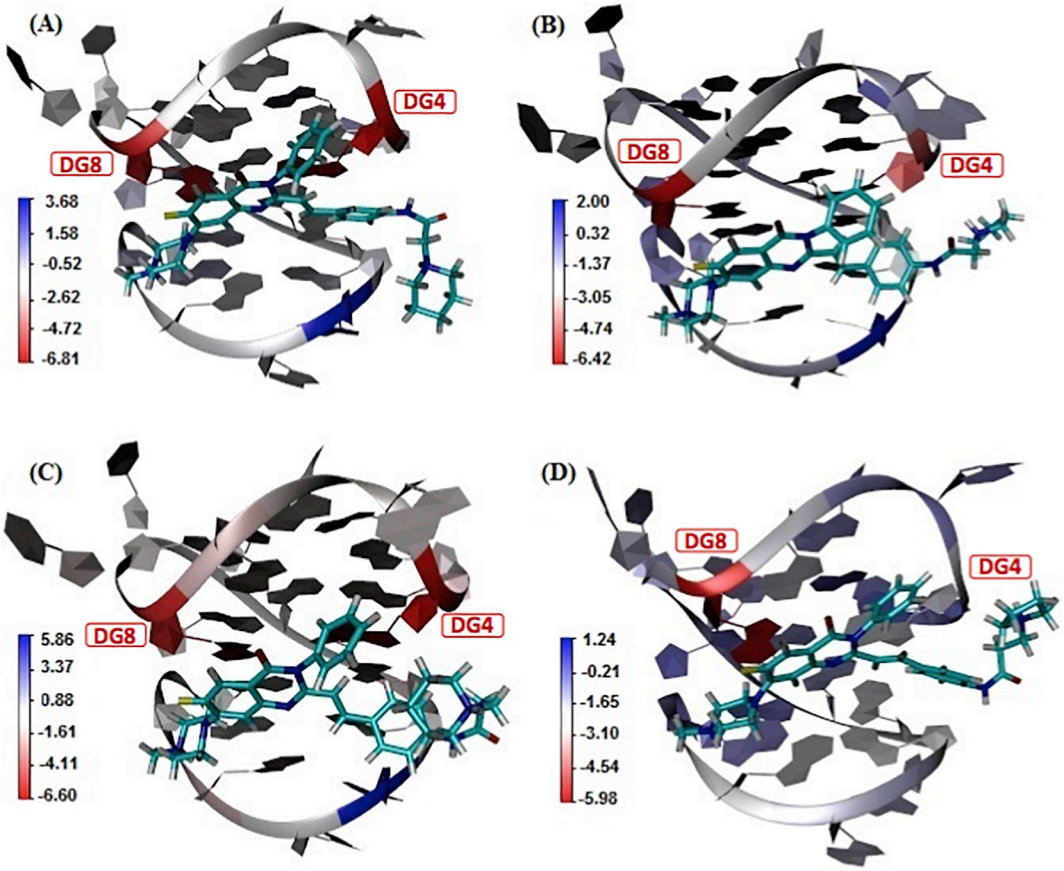

Fig. 10. The mapping of G-quadruplex-ligand complex energy contribution. (A) QD1, (B) QD2, (C) QD3, (D) QD4 complexes. The colour scale bar represents the variation of total free energy for the residues (in kcal/mol). (For interpretation of the references to color in this figure legend, the reader is referred to the web version of this article.)

(ΔG_{bind}) suggesting that all ligands can stabilize c-KIT G-quadruplex. Clearly, different substituents at the side chain of ligands present different stabilizing effects onto c-KIT G-quadruplex. A comparison between QD1 and QD2 shows that despite of the fact that the nonpolar contribution to the binding free energy ($\Delta G_{nonpolar}$) as well as electrostatic interaction energy (ΔE_{elec}) are more negative for QD2 compared to QD1 (−58.3 kcal/mol vs. −55.6 kcal/mol and − 96.7 kcal/mol vs. −93.8 kcal/mol for $\Delta G_{nonpolar}$ and ΔE_{elec}, respectively), QD1 forms slightly a more stable G-quadruplex-ligand complex than QD2 (−44.2 vs. −42.7 kcal/mol). This can be attributed

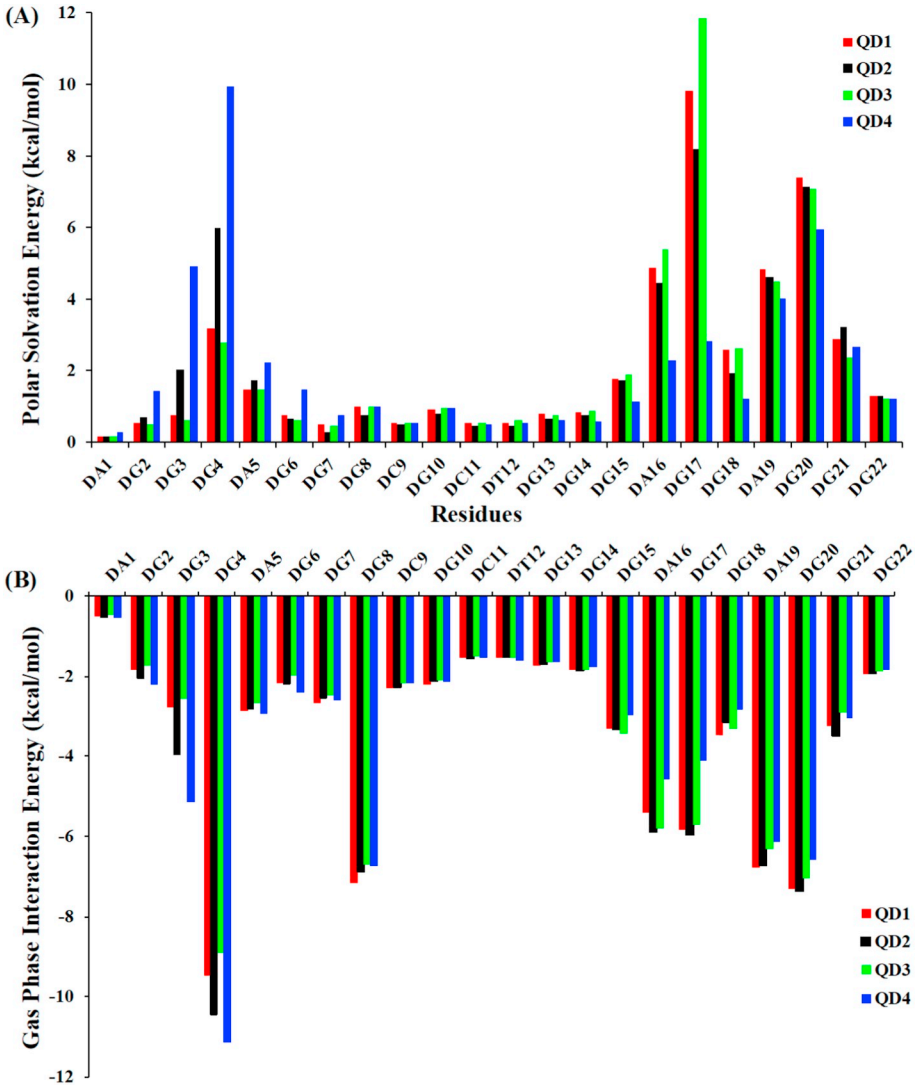

Fig. 11. Decomposition of polar solvation energy (A) and gas phase energy (B) on a per residue level for the complexes. Red: QD1, black: QD2, green: QD3 and blue: QD4. (For interpretation of the references to colour in this figure legend, the reader is referred to the web version of this article.)

to the fact that the ligand QD1 forms two hydrogen bonds with G-quadruplex whereas the ligand QD2 forms 4 hydrogen bonds, that leads to the less negative ΔE_{elec} (−93.8 vs. −96.7 kcal/mol) and consequently to a decrease in unfavorable polar solvation energy (105.2 vs. 112.2 kcal/mol), thereby providing more negative binding free energy in comparison with QD2. The similar trend is observed when one compares QD3, that forms two hydrogen bonds with G-quadruplex, with QD4 that forms four hydrogen bonds with G-quadruplex. Although the QD3 complex has less negative electrostatic and van der Waals energies than QD4 complex, its less unfavorable polar solvation energy leads ultimately to the more negative binding free energy, making the QD3 complex slightly more stable than QD4 complex (−40.0 vs. −38.8 kcal/mol). However, comparing the ΔG_{bind} for the ligands that form the same number of hydrogen bonds with G-quadruplex (QD1 with QD3 and QD2 with QD4) shows that the nonpolar contribution to the binding free energy, that is mainly attributed to van der Waals (π-π stacking) interactions, determines the most stable complex, e.g. QD1 being more stable than QD3 and QD2 being more stable than QD4.

In general, by comparing two ligands with different number of hydrogen bonds we observed that the hydrogen bonds between ligands and G-quadruplex can influence the solvation energy and consequently the stability of G-quadruplex. Moreover, when two ligands have the same number of hydrogen bonds, the nonpolar energy contribution of binding free energy which is mainly attributed to van der Waals (π-π stacking) interactions, plays a significant role in G-quadruplex stability.

3.5. Identifying two hotspots for G-quadruplex-ligand interactions

In order to explore which residues of c-KIT G-quadruplex play major roles in ligand binding, the binding free energy of each complex estimated by MM-PBSA approach was decomposed to individual residues of G-quadruplex. The obtained results for all complexes are illustrated in Figs. 9 and 10. It can be seen that the binding interactions between 4-quinazolinone derivatives and c-KIT G-quadruplex are mainly attributed to two hotspot residues including DG4 and DG8 (red colored residues in Figs. 10 and 8). This is explained by the fact that ligands can effectively interact with DG4 and DG8 located at G-quartet 3 (see Fig. 8). Indeed, residue DG4 and DG8 are contributing in π-π stacking interactions with ligands with the exception of DG4 for QD4. As it can be seen in Fig. 9, ligand QD4 has lower binding free energy contribution in residue DG4 compared to other ligands. As it is depicted in Fig. 6, the phosphate oxygen atom of the DG4 residue in G-quadruplex forms a hydrogen bond with the nitrogen atom of pyrrolidino ring of QD4 (O2P…H-N41). The formation of the latter hydrogen bond interferes with the π-π stacking interactions with the DG4 residue and this is

indeed reflected in lower binding free energy contribution for this residue.

In order to obtain in-depth understanding of the effect of ligand substituents on the binding free energy components, the gas phase interaction (electrostatic and van der Waals) and polar solvation energies for all complexes were further decomposed at the residue level and plotted in Fig. 11. As can be observed in Fig. 11A, the residues located at the loop of G-quadruplex structure e.g. DA16, DG17, DA19 and DG20 have higher polar solvation energy contributions compared to other residues. Furthermore, residue DG4 especially for QD4 has high unfavorable polar solvation energy contribution. The latter can be explained by the results obtained from hydrogen bond analysis (section 3.3.); it was observed that only QD4 forms a hydrogen bond with the phosphate group of DG4 residue, i.e. O2P…H-N41, and this leads to higher polar solvation energy contribution of this residue compared to other ligands.

In addition, Fig. 11B shows the gas phase interaction energies for all residues of G-quadruplex in complex with ligands. Note that the gas phase interaction energy is sum of electrostatic and van der Waals energies. For the residue DG4, the gas phase interaction energy contributions of QD1, QD2 and QD3 are large enough to offset the unfavorable polar solvation contributions. Therefore, DG4 has a notable contribution to binding free energy for these three ligands (see Fig. 9). However, in the case of QD4, the observed large contribution of the gas phase interaction energy and the large polar solvation energy for the DG4 residue, do not speak in favor of each other and eventually lead to a lower binding free energy contribution of residue DG4 for ligand QD4 compared to other ligands (see Fig. 9). In addition, residue DG8 has high gas phase interaction energy while it shows a low unfavorable polar solvation energy for all ligands. This can be explained by the fact that this residue is mainly involved in van der Waals interactions, i.e. π-π stacking interactions, rather than the electrostatic interactions, which is in agreement with the previous results. In fact the right balance between electrostatic, van der Waals and polar solvation energies leads to the high contribution of this residue in ligands binding free energy (see Fig. 9) and make this residue a crucial hotspot for the interaction of the G-quadruplex with all the ligands investigated here.

4. Conclusions

In this study, the binding mechanisms of 4-quinazolinone derivatives to c-KIT G-quadruplex were investigated using molecular docking, MD simulations, free energy calculations and free energy decomposition analysis. From docking simulations, the G-quartet 3 is identified as the most energetically favorable binding site for the all 4-quinazolinone ligands. The MD simulations revealed that the 4-quinazolinone family of ligands considered here, that possess a planar aromatic core and two cationic side chains, not only interact with the G-quartet 3 plate via π-π stacking interaction, but also their cationic side chains can interact with the G-quadruplex loop via hydrogen bond interaction. However, neither of these two interactions alone determines the stability of the G-quadruplex-ligand complexes; it is the balance achieved by what is effectively a combination of these interactions. The calculated binding free energies disclosed that ligand QD1 with a short side chain and a terminal piperidino group stabilizes c-KIT G-quadruplex slightly more compared to other derivatives. We found that the modification of side chains of 4-quinazolinone does not necessarily increase the stability of the G-quadruplex via hydrogen bonding. The binding free energy decomposition results demonstrate the crucial roles of two hot spot residues (DG4 and DG8) for the binding of ligands to c-KIT G-quadruplex which is mainly attributed to π-π stacking interactions, highlighting the importance of the planar aromatic moiety of ligands in G-quadruplex stabilization. In summary, we suggest that increasing the planarity and aromaticity of 4-quinazolinone derivatives, instead of increasing the length of their side chains, that leads to a more stable G-quadruplex-ligand π-π stacking interactions, can serve as a novel strategy to design new G-quadruplex stabilizer with high binding affinity.

Acknowledgments

We would like to thank Dr. Hashemianzadeh for valuable discussion and the Center for Information Technology of the University of Groningen for their support and for providing access to the Peregrine high performance computing cluster.

Appendix A. Supplementary data

Supplementary data to this article can be found online at https://doi.org/10.1016/j.bpc.2019.106220.

References

[1] V.S. Chambers, G. Marsico, J.M. Boutell, M. Di Antonio, G.P. Smith, S. Balasubramanian, Nat. Biotechnol. 33 (2015) 877–881.
[2] D. Rhodes, H.J. Lipps, Nucleic Acids Res. 43 (2015) 8627–8637.
[3] Y. Wu, R.M. Brosh, FEBS J. 277 (2010) 3470–3488.
[4] S. Neidle, Curr. Opin. Struct. Biol. 19 (2009) 239–250.
[5] S. Neidle, S. Balasubramanian, Quadruplex Nucleic Acids, RSC, Cambridge, U.K., 2006.
[6] H. Fernando, A.P. Reszka, J. Huppert, S. Ladame, S. Rankin, A.R. Venkitaraman, S. Neidle, S. Balasubramanian, Biochemistry 45 (2006) 7854–7860.
[7] S. Rankin, A.P. Reszka, J. Huppert, M. Zloh, G.N. Parkinson, A.K. Todd, S. Ladame, S. Balasubramanian, S. Neidle, J. Am. Chem. Soc. 127 (2005) 10584–10589.
[8] S. Sakurai, T. Fukasawa, J.M. Chong, A. Tanaka, M. Fukayama, Jpn. J. Cancer Res. 90 (1999) 1321–1328.
[9] K.S. Smalley, K.L. Nathanson, K.T. Flaherty, Cancer Res. 69 (2009) 3241–3244.
[10] D. Wei, J. Husby, S. Neidle, Nucleic Acids Res. 43 (2014) 629–644.
[11] R. Rocca, F. Moraca, G. Costa, C. Talarico, F. Ortuso, S. Da Ros, G. Nicoletto, C. Sissi, S. Alcaro, A. Artese, ACS Med. Chem. Lett. 9 (2018) 848–853.
[12] S. Balasubramanian, L.H. Hurley, S. Neidle, Nat. Rev. Drug Discov. 10 (2011) 261–275.
[13] Z.A. Waller, S.A. Sewitz, S.T.D. Hsu, S. Balasubramanian, J. Am. Chem. Soc. 131 (2009) 12628–12633.
[14] J. Dash, P.S. Shirude, S.T.D. Hsu, S. Balasubramanian, J. Am. Chem. Soc. 130 (2008) 15950–15956.
[15] K. Jantos, R. Rodriguez, S. Ladame, P.S. Shirude, S. Balasubramanian, J. Am. Chem. Soc. 128 (2006) 13662–13663.
[16] M. Bejugam, S. Sewitz, P.S. Shirude, R. Rodriguez, R. Shahid, S. Balasubramanian, J. Am. Chem. Soc. 129 (2007) 12926–12927.
[17] A. Chauhan, S. Paladhi, M. Debnath, S. Mandal, R.N. Das, S. Bhowmick, J. Dash, Bioorg. Med. Chem. 22 (2014) 4422–4429.
[18] C.W. Ong, M.C. Liu, K.D. Lee, K.W. Chang, Y.T. Yang, H.W. Tung, K.R. Fox, Tetrahedron 68 (2012) 5453–5457.
[19] S. Manaye, R. Eritja, A. Aviñó, J. Jaumot, R. Gargallo, BBA-Gen. Subjects, vol. 1820, (2012), pp. 1987–1996.
[20] M. Bejugam, M. Gunaratnam, S. Müller, D.A. Sanders, S. Sewitz, J.A. Fletcher, S. Neidle, S. Balasubramanian, ACS Med. Chem. Lett. 1 (2010) 306–310.
[21] K.I. McLuckie, Z.A. Waller, D.A. Sanders, D. Alves, R. Rodriguez, J. Dash, G.J. McKenzie, A.R. Venkitaraman, S. Balasubramanian, J. Am. Chem. Soc. 133 (2011) 2658–2663.
[22] J. Dash, R. Nath Das, N. Hegde, G.D. Pantoş, P.S. Shirude, S. Balasubramanian, Chem. Eur. J. 18 (2012) 554–564.
[23] D.M. Răsădean, B. Sheng, J. Dash, G.D. Pantoş, Chem. Eur. J. 23 (2017) 8491–8499.
[24] M.C. Nielsen, A.F. Larsen, F.H. Abdikadir, T. Ulven, Eur. J. Med. Chem. 72 (2014) 119–126.
[25] K.V. Diveshkumar, S. Sakrikar, S. Harikrishna, V. Dhamodharan, P.I. Pradeepkumar, Chem. Med. Chem. 9 (2014) 2754–2765.
[26] H. Jin-Qiang, J.H. Tan, X.X. Wang, S.B. Chen, S.Y. Huang, J.W. Yan, S.H. Chen, T.M. Ou, H.B. Luo, D. Li, L.Q. Gu, Z.S. Huang, Org. Biomol. Chem. 9 (2011) 6422–6436.
[27] X. Wang, C.X. Zhou, J.W. Yan, J.Q. Hou, S.B. Chen, T.M. Ou, L.Q. Gu, Z.S. Huang, J.H. Tan, ACS Med. Chem. Lett. 4 (2013) 909–914.
[28] K.G. Moghaddam, S.M. Hashemianzadeh, RSC Adv. 5 (2015) 76642–76650.
[29] B. Machireddy, G. Kalra, S. Jonnalagadda, K. Ramanujachary, C. Wu, J. Chem. Inf. Model. 57 (2017) 2846–2864.
[30] A. Spinello, G. Barone, J. Grunenberg, Phys. Chem. Chem. Phys. 18 (2016) 2871–2877.
[31] Z. Shen, K.A. Mulholland, Y. Zheng, C. Wu, J. Mol. Model. 23 (2017) 256–267.
[32] S. Sillapapongwarakorn, S. Yanarojana, D. Pinthong, A. Thithapandha, J. Ungwitayatorn, P. Supavilai, Bioinformation 13 (2017) 284–292.
[33] M.J. Frisch, G.W. Trucks, H.B. Schlegel, G.E. Scuseria, M.A. Robb, J.R. Cheeseman, J.A. Montgomery, T. Vreven Jr., K.N. Kudin, J.C. Burant, et al., Gaussian 03, Gaussian, Inc., Wallingford, CT, 2004.
[34] O. Trott, A.J. Olson, J. Comput. Chem. 31 (2010) 455–461.
[35] M.F. Sanner, J. Mol. Graph. Mod. 17 (1999) 57–61.
[36] D. Van Der Spoel, E. Lindahl, B. Hess, G. Groenhof, A.E. Mark, H.J.C. Berendsen, J. Comput. Chem. 26 (2005) 1701–1718.
[37] A.W. Sousa da Silva, W.F. Vranken, BMC Res. Notes, vol. 23, (2012), pp. 367–375.
[38] A. Pérez, I. Marchán, D. Svozil, J. Sponer, T.E. Cheatham, C.A. Laughton,

M. Orozco, Biophys. J. 92 (2007) 3817–3829.
[39] J. Wang, R.M. Wolf, J.W. Caldwell, P.A. Kollman, D.A. Case, J. Comput. Chem. 25 (2004) 1157–1174.
[40] D.J. Price, C.L. Brooks III, J. Chem. Phys. 121 (2004) 10096–10103.
[41] G. Bussi, D. Donadio, M. Parrinello, J. Chem. Phys. 126 (2007) 014101–014107.
[42] M. Parrinello, A. Rahman, J. Appl. Phys. 52 (1981) 7182–7190.
[43] S. Nosé, M.L. Klein, Mol. Phys. 50 (1983) 1055–1076.
[44] T. Darden, D. York, L. Pedersen, J. Chem. Phys. 98 (1993) 10089–10092.
[45] B. Hess, H. Bekker, H.J.C. Berendsen, J.G. Fraaije, J. Comput. Chem. 18 (1997) 1463–1472.
[46] X. Daura, K. Gademann, B. Jaun, D. Seebach, W.F. Van Gunsteren, A.E. Mark Angew, Chem 38 (1999) 236–240.
[47] W. Humphrey, A. Dalke, K. Schulten, J. Mol. Graph. 14 (1996) 33–38.
[48] E.F. Pettersen, T.D. Goddard, C.C. Huang, G.S. Couch, D.M. Greenblatt, E.C. Meng, T.E. Ferrin, J. Comput. Chem. 25 (2004) 1605–1612.
[49] P.A. Kollman, I. Massova, C. Reyes, B. Kuhn, S. Huo, L. Chong, M. Lee, T. Lee, Y. Duan, W. Wang, O. Donini, P. Cieplak, J. Srinivasan, D.A. Case, T.E. Cheatham, Acc. Chem. Res. 33 (2000) 889–897.
[50] N. Homeyer, H. Gohlke, Mol. Inf. 31 (2012) 114–122.
[51] S. Harikrishna, S. Kotaru, P.I. Pradeepkumar, Mol. BioSys. 13 (2017) 1458–1468.
[52] K. Rashmi, R. Kumar, A. Lynn, J. Chem. Inf. Model. 54 (2014) 1951–1962.
[53] M.K. Gilson, B. Honig, Proteins 4 (1988) 7–18.
[54] S.W. Clark, A. Tempczyk, R.C. Hawley, T. Hendrickson, J. Am. Chem. Soc. 112 (1990) 6127–6129.
[55] H. Barry, A. Nicholls, Science 268 (1995) 1144–1149.
[56] N.A. Baker, D. Sept, S. Joseph, M.J. Holst, J.A. McCammon, Proc. Natl. Acad. Sci. U. S. A. 98 (2001) 10037–10041.
[57] S. Jayashree, T.E. Cheatham, P. Cieplak, P.A. Kollman, D.A. Case, J. Am. Chem. Soc. 120 (1998) 9401–9409.
[58] S. Doree, K.A. Sharp, B. Honig, J. Phys. Chem. 98 (1994) 1978–1988.
[59] S. Genheden, U. Ryde, Expert Opin. Drug Discovery 10 (2015) 449–461.
[60] J. Srinivasan, T.E. Cheatham, P. Cieplak, P.A. Kollman, D.A. Case, J. Am. Chem. Soc. 120 (1998) 9401–9409.
[61] D. Shi, Q. Bai, S. Zhou, X. Liu, H. Liu, X. Yao, Proteins 86 (2018) 43–56.
[62] A.T. Phan, V. Kuryavyi, S. Burge, S. Neidle, D.J. Patel, J. Am. Chem. Soc. 129 (2007) 4386–4392.
[63] A. Głuszyńska, B. Juskowiak, M. Kuta-Siejkowska, M. Hoffmann, S. Haider, Molecules 23 (2018) 1134–1154.
[64] H. Berk, J. Chem. Phys. 116 (2002) 209–217.